

3D FINITE ELEMENT MODELING OF SINGLE-LAP SHEAR BOLTED JOINTS

Alex Selvarathinam*, James Frailey*, Jim Eisenmann**
***Lockheed Martin Aeronautics, CAE Development and Support,**
Lockheed Martin Aeronautics (Retired)**

Keywords: *Single-Lap, finite element, beam on elastic foundation, bolted joint*

Abstract

A comprehensive 3D finite element study of a single-lap shear bolted joint was undertaken and the analysis results were compared with normalized test data and subsequently employed to validate beam on elastic foundation analysis. Good correlation with experimental data (within certain load range) and beam on elastic foundation results was obtained.

1 Introduction

Since bolted joints are used extensively in aircraft primary and secondary structure, it is essential to design the joints correctly to transfer loads efficiently and to minimize the overall weight of the aircraft. Some of the key areas where bolted joints find use include aircraft wing, tail and control surfaces.

A critical drawback of bolted joints is they interrupt the continuity of geometry and therefore are locations of high stress concentrations. The stress state in the bolted joint is further complicated by the presence of material anisotropy as is the case for composite materials joints. This complex stress state has been the cause of several failures in aircraft and continues to be an area of active research in academia and industry [1]-[2].

The complex stress state existing in composite bolted joints has been studied extensively using 2D finite element analysis (FEA) in the past [3]-[6] and more recently using 3D FEA [7]-[8]. These studies ([1]-[9]) supported by experimental data have improved the understanding of stress state in bolted joints significantly. However, the complexity of the

finite element model and the computational time required severely limit the usefulness of the complex models in a production environment. The afore-mentioned model, though, serve as a useful tool for validating simpler closed form solutions that are typically used in production. The complexity of the FEA model arises due to the diverse failure modes, material and geometric non-linearity, and the contact surfaces that have to be modeled to obtain results that track experimental data reasonably well. Therefore, typically a global FEA model without the afore-mentioned complexities is used to derive loads near the joints. Then closed form solutions are employed to get detailed local stress state in the joint using the results from the global FEA model.

At Lockheed Martin Aeronautics detailed stress analysis tools that are used for both fastener analysis and bolted joint analysis employ the 2D beam on elastic analysis foundation method (BEF) [10] to resolve loading along the axis of the fastener and bearing loads acting on the fastener hole.

1.1 Beam on Elastic Foundation (BEF) Method

A schematic of the joint configuration assumed for the BEF analysis, the relation to the actual configuration, and the results obtained from the analysis are shown in Fig. 1.

The BEF analysis is typically used to determine the shear and moment distribution along the fastener axis and the peak bearing stress due to the interaction between the fastener hole and the fastener as shown in Fig. 1.

Empirically derived parameters, based on element and component level testing, are included in the BEF analysis in the form of head and nut fixity values and the foundation modulus. The accuracy of the BEF analysis in determining the shear and moment distribution along the fastener axis and peak bearing stress has not previously been verified and therefore it was decided to validate the BEF results with a detailed 3D FEA.

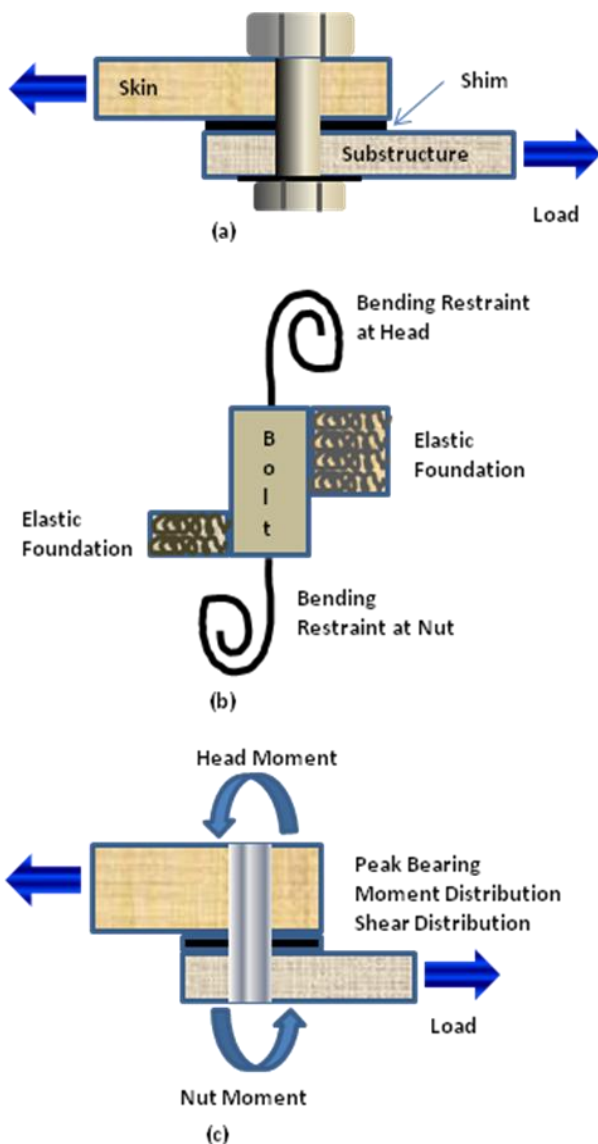


Fig. 1 Schematic of BEF. (a) Actual Joint (b) BEF model (c) Analysis Results

2 Motivation

The primary motivation for performing this study was born out of the need to validate the

afore-mentioned simple 2D BEF method [10] employed at Lockheed Martin Aeronautics to analyze fasteners and bearing loads. The validation was performed by comparing the BEF results with a comprehensive 3D FEA where failure initiation and progressive material degradation in the composite materials were explicitly modeled. It is not our objective here to discuss or study the diverse and complex nature of bolted-joint failure mechanisms. However for those interested in such there is an extensive body of literature available [1]-[6].

Typically there are several thousand fasteners distributed over the primary and secondary aircraft structures. For example the Joint Strike Fighter has over 6000 fasteners in the wing skin alone that have to be analyzed. Each bolted joint is analyzed using computationally efficient detail stress tools employing the BEF method. The detail stress analysis is achieved by first developing a medium or fine grid finite element mesh of the aircraft part. Fasteners are modeled discretely; for example, using NASTRAN [12] CBUSH elements. The nodal forces and moments at the fastener location are extracted from the fastener elements and subsequently used as inputs to the BEF analysis to size the aircraft parts.

Guided by the foregoing objectives a comprehensive 3D FEA of a single lap shear joint was undertaken and the results compared with (i) test data and (ii) the results of a 2D BEF analysis. The purpose for comparing the FEA results with test data was to ensure that the model captured the general trend of the test data. The material non-linearity of the fastener, the shear non-linearity of the composites and the geometric non-linearity of the joint were modeled. Furthermore, tension, compression and shear failure modes were included in the analysis. Since the focus of the present study is to compare the BEF with a rigorous 3D FEA the progressive damage material model will not be discussed in detail here.

The study compared the bending moment and shear force variations along the fastener axis, and the peak bearing stress predicted by the 3D FEA with the BEF results. Furthermore the effect of friction on load transfer paths

through the fastener and the laminates was assessed.

3 Test Coupon Description

The test coupon geometry is shown in Fig. 2. Test coupons consisted of a head plate (skin) and a tail plate (substructure) separated by a shim. A series of six fasteners attached the three layers together. Load blocks were attached to the head and tail plates to transfer load through the center of the joint. Furthermore, there were four stabilizing rods (shown later) that restrained the rotation of the plates.

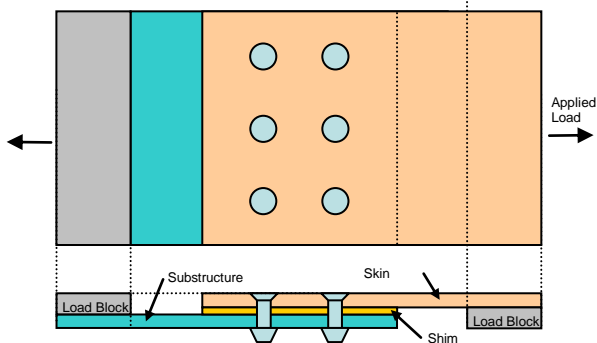


Fig. 2 Test Coupon Geometry.

4 Finite Element Scheme

ABAQUS V6.8 [13] was employed to perform the 3D detailed FEA in this study due to its proven nonlinear capability. Due to the symmetry of the problem only one row of fasteners was modeled. ABAQUS single order brick (C3D8) and wedge (C3D6) elements were used throughout the model. The FEA model was generated using PATRAN PCL script. The geometric inputs that could be varied in the script are shown in Fig. 3. However for this study all the variables matched the test specimen. For the purpose of brevity the geometric inputs are not provided in this paper.

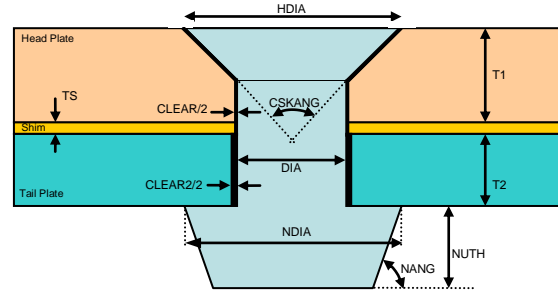


Fig. 3 Fastener Model Variables

The model was designed to accommodate a separate diametric hole clearance for the head and tail plates. However, a single value was used as clearance for this study. The fastener and nut were modeled as a single solid member with Titanium elastic-plastic material properties.

4.1 Skin & Substructure

The skin was modeled with 3792 hex elements as shown in the following isometric section cut (Fig. 4). The skin mesh was designed to have the same refinement around the fastener hole circumference as the fasteners.

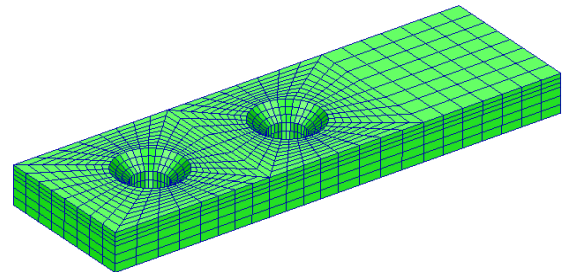


Fig. 4 Skin Mesh with 3792 Hex Elements

Similarly the substructure mesh (Fig. 5) consisting of 2672 hex elements was also designed to match the fastener mesh refinement.

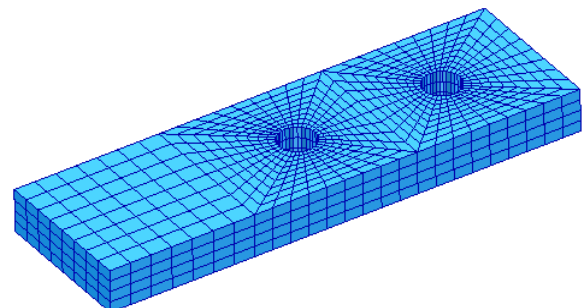


Fig. 5 Substructure Mesh with 2672 Hex Elements

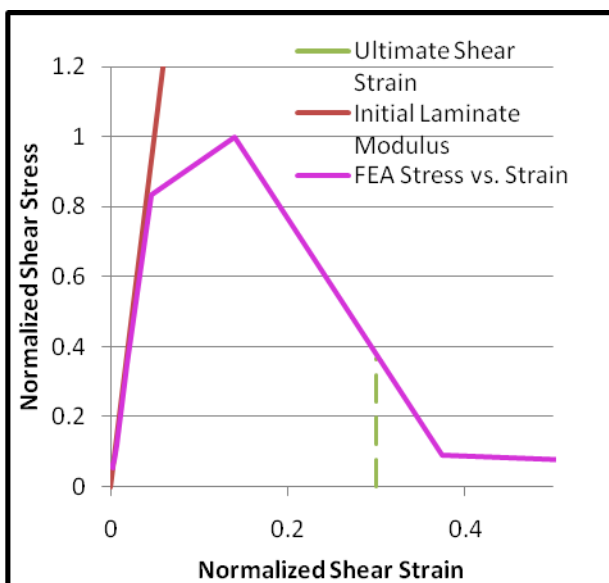
4.2 Composite Material Model

Effective 3D homogeneous orthotropic material properties for the skin and substructure made of Carbon/Bismaleimide IM7/5250 tape/fabric were employed in this study. The skin and substructure were each made of 34 plies with a laminate stacking sequence of $[45_2/90/-45/0/45/90/-45/0/45/90/-45/0/45/90/-45/0]_s$.

4.2.1 Composite Non-linear Shear Model

Only G_{12} , the effective laminate shear modulus in the 1-2 loading plane, was assumed to be non-linear since loading was primarily in the 1-2 plane. Usually the shear non-linearity is modeled using the Hahn and Tsai [11] model based on complementary energy density. However, in the current study, to keep the analysis simple, the non-linear shear damage was approximated using an exponential function similar to that used by Hung and Chang [6] to model shear modulus degradation. This results in the shear stress/strain behavior as depicted in Fig. 6. The exponential degradation function not only models the effect of non-linearity but also causes gradual reduction in stresses prior to failure initiation alleviating numerical instabilities. Subsequent to failure initiation at ultimate shear strain the material degradation rule described in the next section, takes over.

The shear non-linearity was modeled in FEA using the user defined field variable subroutine available in ABAQUS [13].



Copyright © 2010 by Lockheed Martin Corporation

Fig. 6 The Non-Linear Shear Stress Vs. Shear Strain Behavior Modeled in FEA.

4.2.2 Composite Material Failure Modes and Criterion

Three key in-plane (1-2 loading plane) failure modes were considered in this study. They are the fiber compression failure, fiber tensile failure and the matrix shear failure.

The strains in the global direction were decomposed into strains along the 0° , $\pm 45^\circ$ and 90° and were subsequently used to determine the failure initiation and progression. The fiber strains were compared to ultimate tensile and compression fiber strains and the shear strains were compared to the matrix ultimate shear strain to determine failure initiation.

4.2.3 Composite Material Degradation Rule

Subsequent to failure initiation the modulus and the Poisson's ratio in all the three principal directions were decreased linearly as a function of the strain as depicted in Fig. 7.

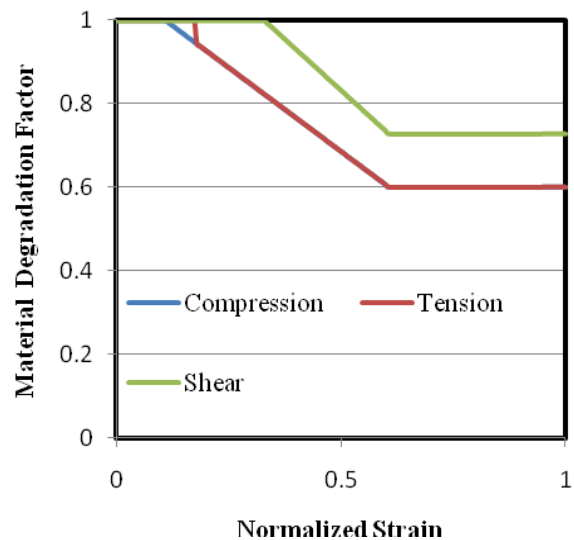


Fig. 7 Material Degradation Factor Model

Once failure initiates the material parameters are gradually reduced to a non-zero constant linearly. This is done primarily to improve the numerical convergence of the solution by avoiding instantaneous changes in properties. Since the material parameters are not reduced to zero the current degradation rule is valid only up to the normalized strain of 1 beyond which gross failure of the joint occurs.

4.3 Fasteners

Each fastener was modeled with 1504 elements (1088 Hex, 416 Wedge). The fasteners were modeled with Titanium elastic-plastic properties using the true stress, true plastic strain of Ti-6Al-4V Alloy [14].

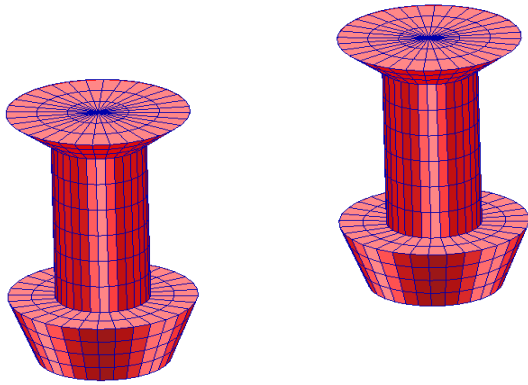


Fig. 8 Fastener Mesh.

A pre-tension force, which is introduced in the fasteners when torqued, was also modeled in the FEA.

4.4 Shim & Stabilizing Rods

The shim was modeled with 576 hex elements as shown in the following isometric section cut (Fig. 9).

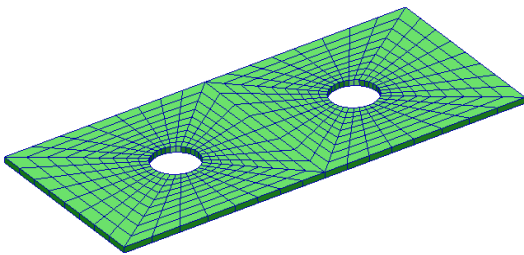


Fig. 9 Shim Mesh with 576 Hex Elements

The shim, which was modeled with linear isotropic aluminum properties, was designed to have the same mesh as the bottom of the head plate.

To prevent undue rotation of the joint during loading, test specimens were restrained by four steel rods with Teflon[®] at their ends. Two stabilizing rods contacted the Head plate and two contacted the Tail plate. The stabilizing rods were fixed in space on the ends away from the joint and contact surfaces were

defined on the other ends. The entire model along with the stabilizing rods is shown in Fig. 10.

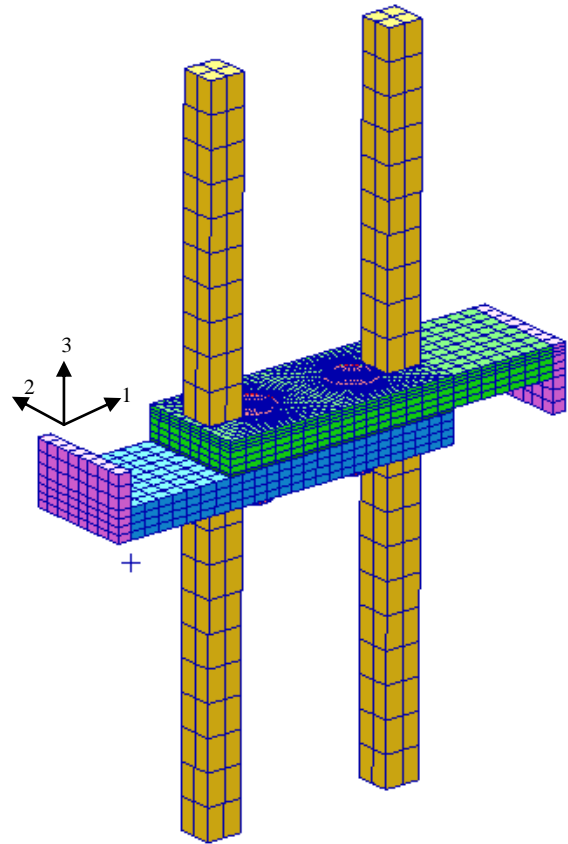


Fig. 10 The 3D FEA Model with the Stabilizing Rods

4.5 Contact Surfaces & Friction

The contact surfaces were defined between 14 pairs: skin-shim, substructure-shim, fasteners (left and right) and skin, fasteners (left and right) and shim, fasteners (left and right) and substructure, nut head (left and right) and substructure, top stabilizing rods (left and right) and skin, and bottom stabilizing rods (left and right) and substructure. A friction coefficient of 0.14 was used on all contact surface pairs except the surfaces between the stabilizing rods and the skin and substructure where the surface friction was reduced to 0.07 because of the presence of Teflon[®]. The contact surface pairs are sketched in Fig. 11.

Pair	
Skin – Shim	
Substructure – Shim	
Fastener Left – Skin	
Fastener Right – Skin	
Fastener Left – Shim	
Fastener Right – Shim	
Fastener Left – Substructure	
Fastener Right – Substructure	
Nut Head Left – Substructure	
Nut Head Right – Substructure	
Stabilizing Rod Top Left – Skin	 Friction coefficient reduced to 0.07 due to Teflon®/composite interface. Same on following three contact pairs.
Stabilizing Rod Top Right – Skin	
Stabilizing Rod Bottom Left – Substructure	
Stabilizing Rod Bottom Right – Substructure	

Fig. 11 Schematic of the 14 Contact Surfaces Pairs used in the 3D FEA Model

Copyright © 2010 by Lockheed Martin Corporation

4.6 Boundary Conditions

The model was fixed by restricting all three translational DOFs on the left surface of the reaction mesh (left in Fig. 12). The bottom surface of the load introduction mesh (right in Fig. 12) was restricted in translational DOFs 2 and 3, both perpendicular to the loading direction. The right surface of the load introduction mesh was given an enforced displacement in the 1 direction as depicted in Fig. 12.

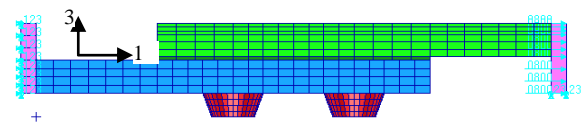


Fig. 12 Boundary Conditions

5 Results

Employing the 3D FEA, the following were studied and the results are presented below: (i) load deflection curve, (ii) moment along the fastener, (iii) shear force along the fastener (iv) peak bearing stress and its location and (v) effect of friction on load transfer. Furthermore items (ii) - (iv) were compared with the result obtained employing 2D BEF analysis.

A portion of the displacement of the 3D finite element model near the fastener is shown magnified in Fig. 13.

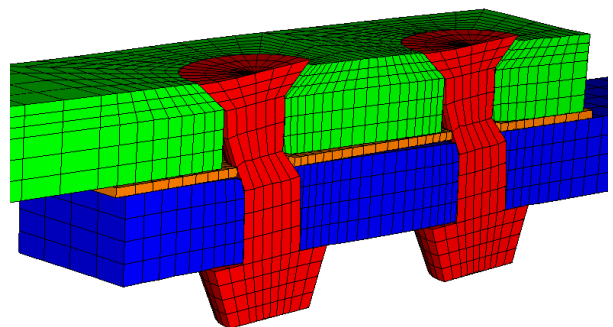


Fig. 13 Magnified Close-up View of the Cross Section of the Deflected Single Lap Shear Joint Near the Fasteners.

5.1 Comparison with Test Data

The displacements in the test joint were measured across a 3 inch span as depicted in Fig. 14.

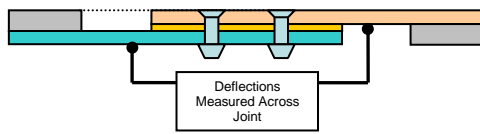


Fig. 14 Joint Deflections Measured Across Three Inch Span

These displacements were compared with the load-deflection curve obtained using the 3D FEA for the three scenarios described in Fig. 16.

Case	Description
Elastic Fastener	Fastener is elastic, composite material is linear with no damage
Not Degraded	Fastener is elastic-plastic, composite material is linear with no damage
Degraded	Fastener is elastic-plastic, composite material is non-linear in shear (1-2 plane only), material failure initiation and damage progression is modeled

Fig. 15 Fastener and Composite Material Models.

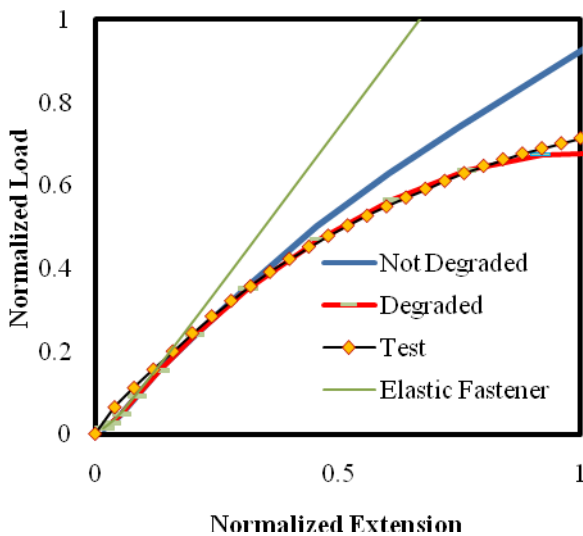


Fig. 16 Comparison of Load-Deflection Test Data with FEA, with and without Degradation Material Model

As can be observed from Fig. 16 the FEA without considering both the fastener plasticity and material degradation grossly overestimated the load deflection curve. However, by including fastener plasticity the FEA results tracks the experiment well until the effects of material non-linearity, failure initiation and

progression sets in. Once the material degradation effect were considered the FEA and the experimental data matched reasonably well up to the point where gross failure occurs in the joint (normalized extension > 1). Past this the FEA model is not accurate as discussed in 4.2.3. Furthermore, modeling the gross failure is beyond the scope of the current study.

5.2 Comparison of Moment Distribution Along the Fastener Shank with BEF

The moment distribution evaluated using the 3D FEA along the fastener axis was compared with the 2D BEF. The moments were compared at two loads, one at 22% (Fig. 17) and another at 72% (Fig. 18) of the ultimate bolt shear load. At 22% ultimate load the fastener is elastic whereas at 72% it has undergone plastic deformation.

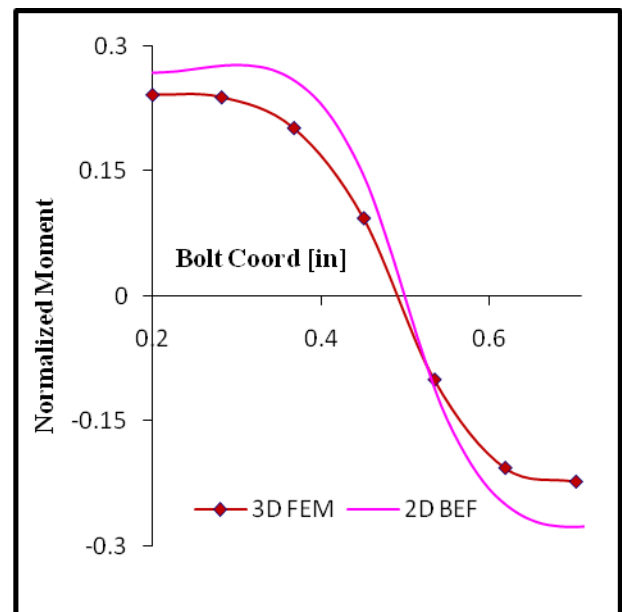


Fig. 17 Moment Distribution Along Fastener Shank at 22% of Ultimate Bolt Shear Load. Fastener Nut is at 0.2 in and Countersink-Shank Intersection is at 0.7 in.

The fastener nut is located at 0.2 and the countersink-shank intersection is located at 0.7. The moment distribution profile and the change in profile due to increased load is captured reasonably well by BEF even in the plastically deformed zone which is not modeled explicitly in the BEF analysis.

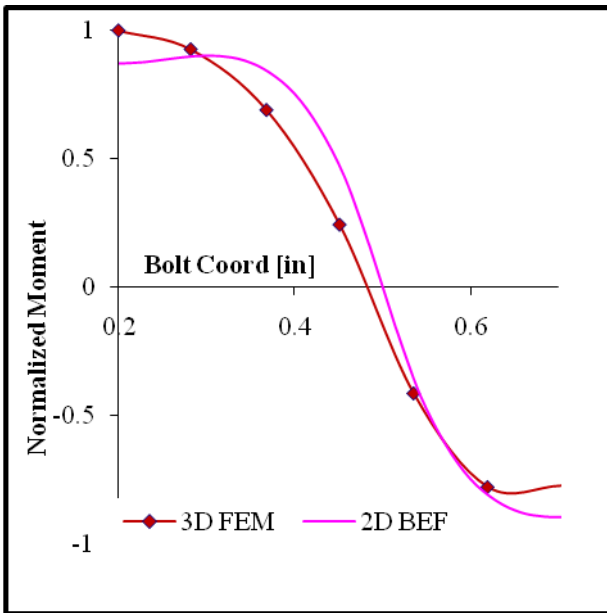


Fig. 18 Moment Distribution Along Fastener Shank at 72% of Ultimate Bolt Shear Load. Fastener Nut is at 0.2 in and Countersink-Shank Intersection is at 0.7in.

5.3 Comparison of Shear Distribution Along Fastener Shank with BEF

The shear force distribution along the fastener shank is shown in Fig. 19 at 22% of ultimate bolt shear load and in Fig. 20 at 72% of ultimate bolt shear load.

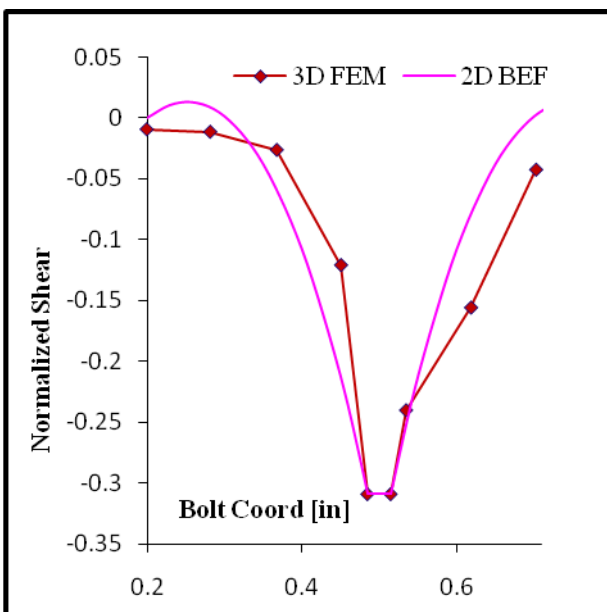


Fig. 19 Shear Force Distribution Along Fastener Shank at 22% of Ultimate Bolt Shear Load. Fastener Nut is at 0.2 in and Countersink-Shank Intersection is at 0.7 in.

From Fig. 19 and Fig. 20 it can be inferred that the BEF analysis captures the shear force distribution reasonably well even when the fastener deforms plastically.

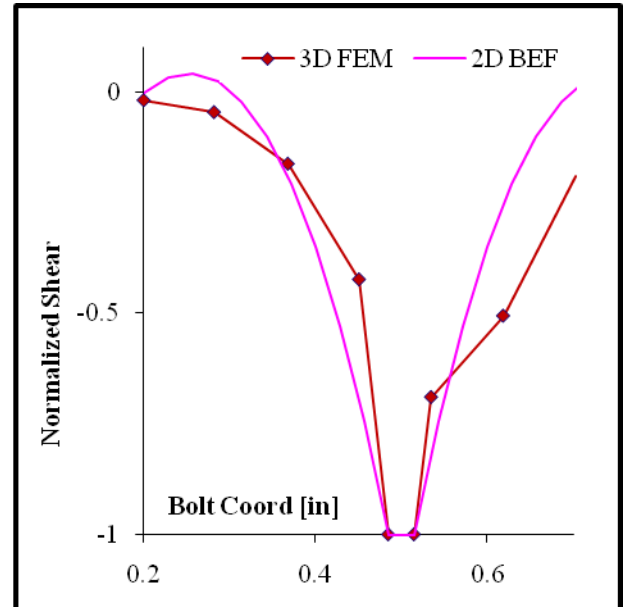


Fig. 20 Shear Force Distribution Along Fastener Shank at 72% of Ultimate Bolt Shear Load. Fastener Nut is at 0.2 in and Countersink-Shank Intersection is at 0.7 in.

5.4 Peak Bearing Stress

The peak bearing stress is defined as the maximum bearing stress between the fastener and fastener hole. The peak bearing stress evaluated using the 3D FEA was compared with the peak bearing stress determined using the 2D BEF analysis in Fig. 21. Higher bearing stress corresponds to increased applied load.

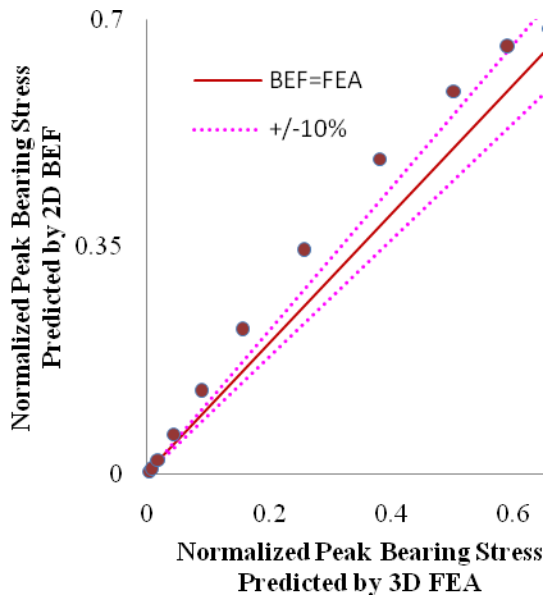


Fig. 21 Comparison of Peak Bearing Stress between the 3D FEA and 2D BEF.

The $\pm 10\%$ scatter band is also shown. From Fig. 21 it can be inferred that BEF analysis again follows the trend predicted by 3D FEA reasonable well.

The fringe plot of bearing stress profile along the fastener as a function of applied load is shown in Fig. 22. As the load increases the maximum bearing stress location shifts from the shank-countersink intersection to close to the middle of the shank where the shim is located. The maximum bearing stress occurs at the same location for BEF analysis also.

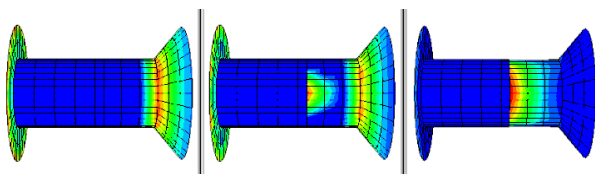


Fig. 22 Progression of Contact Normal Pressure from the Head Towards the Shim on the Side Contacting the Skin as a Function of Applied Load. The Left is at 2%, Middle is at 7% and the Right is at 100% of Applied Maximum Load.

5.5 Effect of Friction on Load Transfer between the Skin and Substructure

The effect of friction on the loads transfer between the skin and substructure was studied.

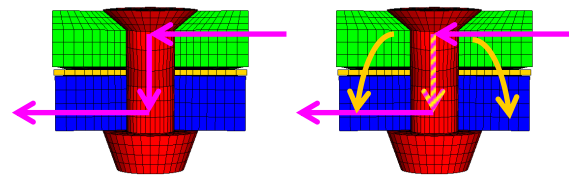


Fig. 23 Load Transfer with Friction Absent (Left) and Friction Present (Right).

For this purpose two cases were considered. In the first case no friction was assumed to act between any contact surfaces including the surfaces in contact with the shim (left in Fig. 23). This case was compared with another where the friction was introduced between all the contact surfaces (right in Fig. 23).

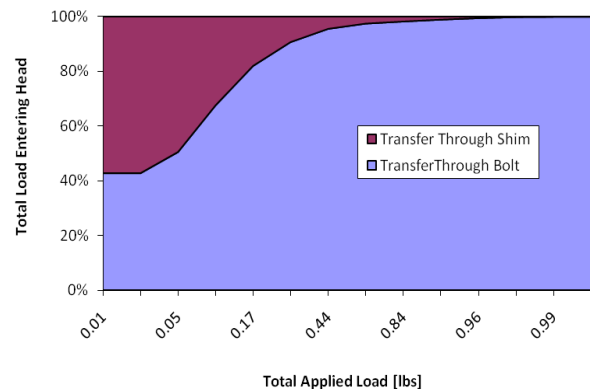


Fig. 24 Variation of Load Transferred through Shim and Bolt as a Function of Applied Load When Friction is Present.

For case 1 the entire load from the skin to the substructure is transferred through the fastener. In case 2 due to friction between the fastener and shim a portion of the load is transferred through the shim as depicted in Fig. 24. From the figure it can be inferred that at lower loads friction plays a role in transferring loads from the skin to the substructure. However for higher loads the effect of friction diminishes. Therefore the aircraft industry's practice of ignoring the beneficial effect of friction seems justified.

6 Conclusions

The load deflection curve of the 3D FEA tracked the test results well up to the point where gross failure of the joint occurs. The study determined that the bending moment and shear force variations along the fastener axis,

and the peak bearing stress predicted by the 3D FEA compared reasonably well with the BEF results. Consequently, the study supports the use of the BEF method to predict loads in bolted joints. Since BEF is computationally efficient relative to 3D FEA, detail stress analysis tools based on BEF may be employed in large-scale batch analysis jobs across several bolted joints and loading conditions.

The effect of friction on load transfer between the skin and substructure was also studied and it was observed that even though friction was a factor in load transfer through the joint at lower loads, the effect of friction diminished at higher loads.

References

- [1] Hart-Smith, L. J. Bolted Joint Analysis for Composite Structures - Current Empirical Methods and Future Scientific Prospects. *Joining and Repair of Composite Structures*, ASTM STP 1455, K.T. Kedward and H. Kim, Ed.(s), ASTM International, West Conshohocken, PA, 2004.
- [2] Oplinger, D. W. Mechanical Fastening and Adhesive Bonding, S. T. Peters (Ed.), *Handbook of Composites*. London: Chapman & Hall, 1998.
- [3] Xiao, Y and Ishikawa, T. Bearing Strength and Failure Behavior of Bolted Composite Joints (Part II: Modeling and Simulation). *Composites Science and Technology*, vol. 65, pp. 1032-1043, 2005.
- [4] Lessard, L.B and Shokrieh, M.M. Two-Dimensional Modeling of Composite Pinned-Joint Failure. *Journal of Composite Materials*, vol. 29, pp. 671-697, 1995.
- [5] Chang, F-K., and L. B. Lessard, Damage Tolerance of Laminated Composites Containing an Open Hole and Subjected to Compressive Loadings: Part I—Analysis. *Journal of Composite Materials*, vol. 25, pp. 2–43, 1991.
- [6] Hung, C and Chang, F. Bearing Failure of Bolted Composite Joints. Part II: Model and Verification. *Journal of Composite Materials*, vol. 30, pp. 1359-1400, 1996.
- [7] Perugin, P., Riccio, A., and Scaramuzzio, F. Three-Dimensional Progressive Damage Analysis of Composite Joints, Proceedings of the Eighth International Conference on Civil and Structural Engineering Computing., Topping B.H.V (Ed.), 2001.
- [8] McCarthy, C.T., M.A. McCarthy, Three-dimensional finite element analysis of single-bolt, single-lap composite bolted joints: Part II - effects of bolt-hole clearance, *Composite Structures*, vol. 71(2), pp. 159-175, 2005.
- [9] Gray, P.J., C.T. McCarthy, A Global Bolted Joint Model for Finite Element Analysis of Load Distribution in Multi-Bolt Composite Joints, *Composites Part B: Engineering*, Vol. 41, pp 317-325, 2010.
- [10] Barrois, W. Stresses and Displacements Due to Load Transfer by Fasteners in Structural Assemblies. *Engineering Fracture Mechanics*, vol. 10, pp. 115-176, 1978.
- [11] Hahn, H.T and Tsai, S.W. Nonlinear Elastic Behavior of Unidirectional Composite Laminate. *Journal of Composite Materials*, vol. 7, pp. 102-117, 1973.
- [12] MSC NASTRAN, MSC Software.
- [13] ABAQUS V6.8, SIMULIA.
- [14] Military Handbook, MIL-HDBK-5J, vol. 2, 2003.

Copyright Statement

The authors confirm that they, and/or their company or organization, hold copyright on all of the original material included in this paper. The authors also confirm that they have obtained permission, from the copyright holder of any third party material included in this paper, to publish it as part of their paper. The authors confirm that they give permission, or have obtained permission from the copyright holder of this paper, for the publication and distribution of this paper as part of the ICAS2010 proceedings or as individual off-prints from the proceedings.